

## Geochemistry, Geophysics, Geosystems

### RESEARCH ARTICLE

10.1002/2015GC006117

#### Key Points:

- Groundwater flow can greatly alter geothermal heat flux under the East Antarctic Ice Sheet
- Porous elastic sediments and rock can increase subglacial water budget during ice retreat
- Groundwater impact areas in East Antarctica coincide with submarine-based ice

#### Supporting Information:

- Supporting Information S1

#### Correspondence to:

B. T. Gooch,  
bgooch@utexas.edu

#### Citation:

Gooch, B. T., D. A. Young, and D. D. Blankenship (2016), Potential groundwater and heterogeneous heat source contributions to ice sheet dynamics in critical submarine basins of East Antarctica, *Geochem. Geophys. Geosyst.*, 17, 395–409, doi:10.1002/2015GC006117.

Received 28 SEP 2015

Accepted 19 JAN 2016

Accepted article online 25 JAN 2016

Published online 14 FEB 2016

## Potential groundwater and heterogeneous heat source contributions to ice sheet dynamics in critical submarine basins of East Antarctica

Brad T. Gooch<sup>1</sup>, Duncan A. Young<sup>1</sup>, and Donald D. Blankenship<sup>1</sup>

<sup>1</sup>Institute for Geophysics, Jackson School of Geosciences, University of Texas, Austin, Texas, USA

**Abstract** We present the results of two numerical models describing contributions of groundwater and heterogeneous heat sources to ice dynamics directly relevant to basal processes in East Antarctica. A two-phase, one-dimensional hydrothermal model demonstrates the importance of groundwater flow in vertical heat flux advection near the ice-bed interface. Typical, conservative vertical components of groundwater volume fluxes (from either topographical gradients or vertically channeled flow) on the order of  $\pm 1\text{--}10 \text{ mm/yr}$  can alter vertical heat flux by  $\pm 50\text{--}500 \text{ mW/m}^2$  given parameters typical for the interior of East Antarctica. This heat flux has the potential to produce considerable volumes of meltwater depending on basin geometry and geothermal heat production. A one-dimensional hydromechanical model demonstrates that groundwater is mainly recharged into saturated, partially porous elastic (i.e., vertical stress only; not coupled to a deformation equation) sedimentary aquifers during ice advance. During ice retreat, groundwater discharges into the ice-bed interface, which may contribute to water budgets on the order of  $0.1\text{--}1 \text{ mm/yr}$ . We also present an estimated map of potentially heterogeneous heat flow provinces using radiogenic heat production data from East Antarctica and southern Australia, calculated sedimentary basin depths, and radar-derived bed roughness. These are overlaid together to delineate the areas of greatest potential effect from these modeled processes on the ice sheet dynamics of the East Antarctic Ice Sheet.

### 1. Observations: General

Recent studies [e.g., Mackintosh *et al.*, 2011; Fretwell *et al.* 2013; Mengel and Levermann 2014; Pollard *et al.*, 2015] have shown the potential instability of the East Antarctic Ice Sheet (see Figure 1 for location) in basins lying well below sea level to represent significant contributions to sea level rise (roughly 20 m). Attempting to model this ice sheet accurately for various purposes (e.g. targeting old ice core sites or simulating future ice sheet behavior) has been a field of active research for some time [Huybrechts and Oerlemans, 1988; Wilch and Hughes, 2000; Pattyn, 2008; Van Liefferinge and Pattyn, 2013; Sun *et al.*, 2014; Pollard *et al.*, 2015]. The specifics of ice sheet dynamics depend on many factors including, but not limited to, solar radiation, precipitation, climate, ocean influences, and bed topography and geology. While surface measurements are easier to obtain compared to the subsurface measurements, the subsurface factors are of great importance to the overall ice sheet's stability [e.g., Blankenship *et al.*, 1986, 1993, 2001; Lowe and Anderson, 2003; Hughes *et al.*, 2011; Thoma *et al.*, 2012; Schroeder *et al.*, 2014]. While a few continental ice sheet models incorporate limited subglacial data and estimations of bed geometry, homogeneous geothermal heat flux, and interfacial water systems (e.g., PISM) [Winkelmann *et al.* [2011], others elements such as groundwater flow, sediment erosion, heterogeneous geothermal heat flux, and poroelastic sediments are rarely incorporated [e.g., Flowers *et al.*, 2005; Pattyn, 2010]. These processes are most likely critical additions needed in ice sheet modeling. This research seeks to investigate the nature of some of these subglacial processes on the East Antarctic Ice Sheet, in particular, groundwater flow and heterogeneous geothermal heat flux (see Figure 1 for the specific area of focus).

#### 1.1. Observations: Geothermal Heat Flux

Geothermal heat flux in East Antarctica has been estimated using various approaches. One approach utilizes global surface wave tomography to extrapolate known surface heat flux measured globally to Antarctica [i.e., Shapiro and Ritzwoller, 2004]. Another approach [Fox Maule *et al.*, 2005] utilizes satellite magnetic data to map the depth to the base of the magnetic crust (i.e., Curie depth or isotherm) in East Antarctica and

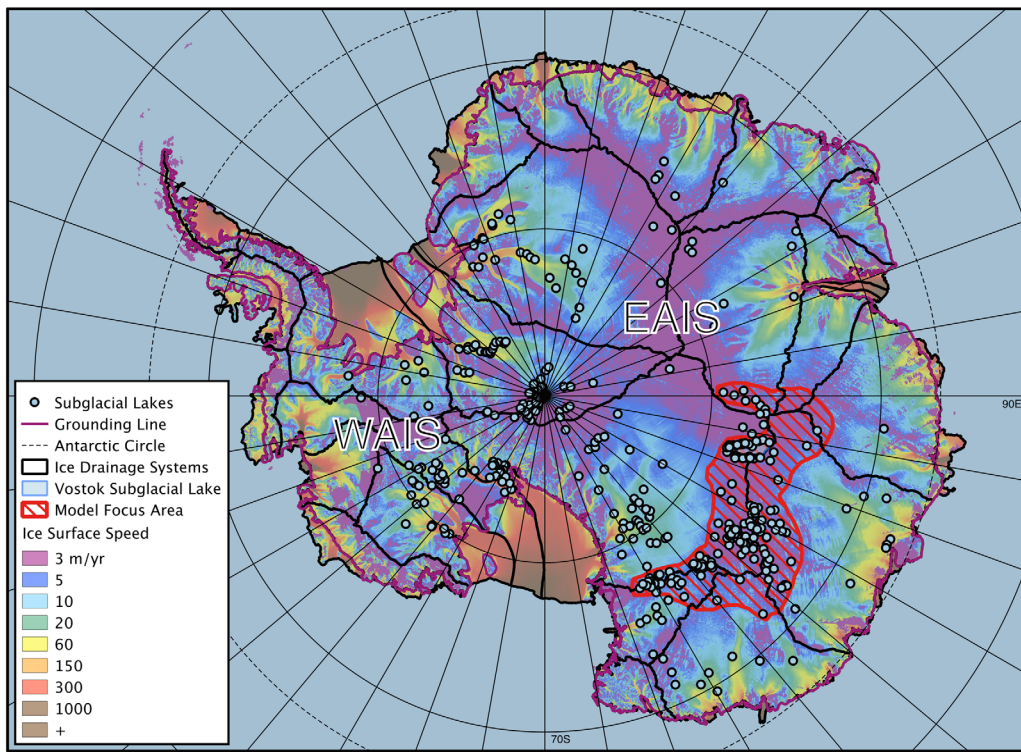


**Figure 1.** Map showing the area of modeling focus and applicability (red-hatched zone). This area was roughly determined by enclosing identified subglacial lakes [Wright and Siegert, 2012] existing under very slow moving ice (surface speed from Rignot *et al.* [2011]) along the ice sheet drainage divides [Zwally *et al.*, 2012] for a large section of East Antarctica known to contain sedimentary basins. The grounding lines used are from Bindschadler *et al.* [2011]. The focus area is used to define typical parameters for the modeling. See section 3 for more details about the model parameters obtained for this area. Note that the latitude and longitude graticules are all in  $10^{\circ}$  increments. The East and West Antarctic Ice Sheet are noted as EAIS and WAIS, respectively.

then model the heat flux from the Curie isotherm to the surface using a very simplified bulk geologic heat transfer model. Yet another approach takes geologic data from Australia and East Antarctica to speculate the heat flux values that may exist using tectonic plate reconstruction [e.g., Pollard *et al.*, 2005]. Pattyn [2010] combined all of those approaches and known subglacial lake distributions to produce a geothermal heat flux map. While none of these approaches has yielded a high-enough resolution estimate of the thermal structure of East Antarctica for adequate ice sheet simulation, they represent the de facto choice for ice sheet modelers until further geologic data is obtained (i.e., thermal properties of the crust such as thermal conductivity and radiogenic heat production).

## 1.2. Observations: Groundwater

The flow of groundwater beneath ice sheets has historically been of interest to glaciologists (see Piotrowski [2006] for review). The importance of groundwater in affecting ice dynamics has been diminished by the glaciological community as an important physical process due to its lack of water transmissivity when compared to the flow of water at the base of the ice (ice-bed interface) [Alley, 1989]. Despite this, many studies have still cited it as a potential cause for concern when modeling cryospheric systems [Clarke *et al.*, 1984; Echelmeyer, 1987; Waddington, 1987; Cutler *et al.*, 2000; Flowers *et al.*, 2005; Boulton, 2010; Christoffersen *et al.*, 2014]. However, there has been a considerable amount of effort to understand how past glaciers and ice sheets affect regional groundwater systems (see Person *et al.* [2012] for review). Many studies have come to the conclusion that ice sheets have reorganized groundwater flow systems and even reversed flow directions [e.g., Grasby *et al.*, 2000; Person *et al.*, 2007; Piotrowski *et al.*, 2009; McIntosh *et al.*, 2011]. Due to the difference in the relax times of the sediments in the upper crust, many groundwater systems previously burdened by ice sheets no longer present still exhibit subsurface pore pressures higher than expected [e.g., Siegel *et al.*, 2014], known as fossil, or anomalous, pore pressure.

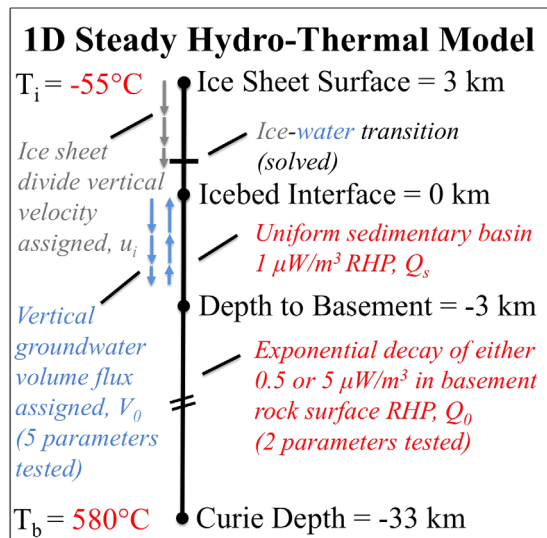


**Figure 2.** Hydrothermal model diagram with explanation. The specific details for this model can be found in section 3.1. “Basement” refers to the crystalline basement rock that exists beneath the modeled sedimentary basin. “RHP” is an abbreviation for the radiogenic heat production (or generation), which naturally occurs from the decay of unstable nuclides in minerals. Note that this vertical heat flow model has two Dirichlet boundary conditions: one at the top and the other at the bottom of the model domain.

of West Antarctica could be the cause for excess basal water. Lemieux et al. [2008a] modeled the groundwater system under the former Canadian Laurentide and found that a great deal of groundwater could be discharged as a result of dwindling ice sheet volumes.

The East Antarctic Ice Sheet (see Figure 1) is a present-day, continental ice sheet that provides an example for study in attempting to answer our hypothesis. While much study has been dedicated to groundwater research in previously glaciated terrains (such as the former Fennoscandian and Laurentide ice sheets), extending this work to a current, continental ice sheet (i.e., East Antarctic Ice Sheet) will provide critical constraints to the impact of groundwater hydrology on basal ice dynamics from subglacial hydrological and geothermal heat flux alteration. The biggest drawback with the East Antarctic example has been the paucity of subsurface data (e.g., hydrogeological or thermal properties) but developments in airborne and satellite remote sensing are improving this situation. Another benefit of the choice of the East Antarctic Ice Sheet for study is that these and other results to follow will help inform ice sheet modelers of previously neglected subglacial processes that may be important for simulations crucial to society’s interest in future sea-level rise prediction and siting of future ice core drilling (frozen ice at the bed is desirable). Current numerical ice sheet models specific to East Antarctic Ice Sheet dynamics do not take into account elevated, heterogeneous geothermal flux at or the presence of groundwater below the ice-bed interface in the sedimentary basins that underlie much of the ice sheet which are below sea level. This is due to the sparse amount of subsurface data below the thick ice sheet but our research will attempt a first pass estimate at the importance of the aforementioned subglacial factors specific to the East Antarctic Ice Sheet.

Our research presented here is divided into three parts. The first two parts are numerical models meant to test the importance of two different basal processes relevant to ice sheet dynamics that are linked to groundwater flow in the subsurface, in particular, those occurring with deep sedimentary basins. The final part represents our analysis of geophysical data to define potential locations of deep sedimentary basins and geochemical data to estimate the range of heterogeneity in radiogenic heat production of the upper East Antarctic crust. Delineating these two basal elements yields areas where our numerically modeled subglacial processes would likely be a significant contributing factor in affecting ice sheet dynamics in East Antarctica. We will demonstrate in this research that understanding these two elements is crucial to better predicting future ice sheet behavior in a rapidly changing climate.

## 2. Hypothesis: Groundwater Flux Impact on East Antarctic Ice Sheet Dynamics

Given that it is well known that ice sheets can affect groundwater systems [e.g., Grasby and Chen, 2005; Bense and Person, 2008; Neuzil, 2015], it is only natural to ask if the reverse is true. Our research here seeks to start answering that question with particular attention to the East Antarctic Ice Sheet. While not being able to fully carry the entirety of basal ice meltwater [Alley, 1989], we hypothesize that groundwater may still be important when coupled to other physical processes connected to ice dynamics such as altering geothermal heat flux or interacting with the water system at the base of the East Antarctic Ice Sheet. For example, Clarke et al. [1984] pointed to groundwater flow as a leading cause for elevated heat flux at the base of Trapridge Glacier in Canada; Echelmeyer [1987] and Waddington [1987] also discussed this topic in greater detail. Christoffersen et al. [2014] discussed the possibility that groundwater in the till underneath ice streams along the Siple Coast

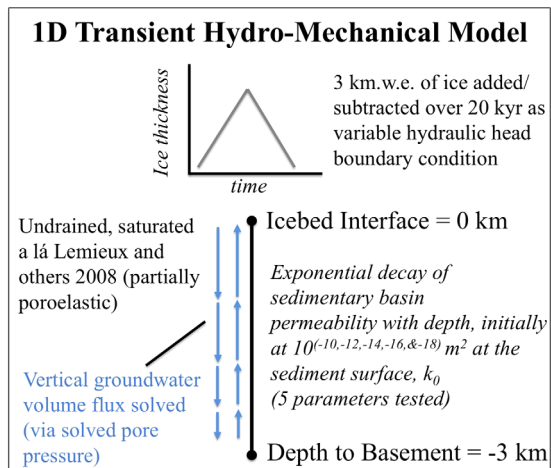


**Figure 3.** Hydromechanical model diagram with explanation. The specific details for this model can be found in section 3.2. Note that the top boundary condition of this vertical groundwater flow model is a variable hydraulic head and the one at the bottom is a no flow boundary condition. Also note that km.w.e. is short for “kilometers water equivalence” in this usage.

models along with their usage references are listed in Table 1. We chose parameters to most conservatively estimate the physical effects at the ice-bed interface whenever possible and are most applicable, but not limited, to the area highlighted in Figure 1.

### 3.1. Experimental Design and Methods: Hydrothermal Model

To test the physical effect of groundwater on East Antarctic Ice Sheet thermal structure, we constructed a steady state, one-dimensional numerical heat transfer model (see Figure 2 for details). The three sections in the model (from deepest to shallowest) are the crystalline basement rock, the sedimentary basin, and finally the ice sheet. The model incorporates conductive heat transfer throughout the domain and couples advective heat transfer in the fully saturated porous media (i.e., sedimentary basin) and ice column. It also allows for the phase change of ice and water in the ice column. The model is one-dimensional for simplicity in order to demonstrate the most straightforward ice physics relationship and to cut down on computational expense. We chose a steady state model to evaluate the magnitude of change in heat vertical heat flux (from groundwater advection and increased heat production) and solved for the basal ice temperatures possible for an example likely to exist in the focus area (likely in a pseudo steady state at present; see Figure 1). We varied the prescribed groundwater volume fluxes [Stauffer, 2006] in both magnitude (decreasing permeability with depth) and direction (i.e., exfiltration or infiltration). Vertical ice flow (downward advection from surface accumulation at ice divides) is kept constant for all model simulations. The ice sheet column is modeled as one being proximal to an ice sheet divide (i.e., lateral ice advection neglected; generally the thickest part of an ice sheet) in order to more clearly elucidate the effects of groundwater-adveected heat flux on the ice sheet thermal state. The governing equations (described below) we used vary along the column depending on the model section component (i.e., where heat is advected or transferred via diffusion only) but are all coupled seamlessly by COMSOL Multiphysics.

The majority of the model domain length extends from the Curie isotherm ( $\sim 580^{\circ}\text{C}$ ) [e.g., Fox Maule *et al.*, 2005], the depth to the base of the magnetic crust, (33 km below the ice bed) to the top of the crystalline basement rock (3 km below the ice bed) that forms the bottom section. These depths, as well as, those in the next section are derived from recent geophysical analyses of East Antarctica [Aitken *et al.*, 2014; Frederick, 2015] as well as drawing on earlier work [Drewry, 1976; Shapiro and Ritzwoller, 2004; Studinger *et al.*, 2004; Fox Maule *et al.*, 2005; Ferraccioli *et al.*, 2009; Jordan *et al.*, 2013]. We chose to rely on a Dirichlet boundary condition (i.e., temperature) at the bottom of the model domain instead of Neumann boundary condition (i.e., heat flux) as a generally known temperature ( $\sim 580^{\circ}\text{C}$ ) exists at a specific estimated depth for the model focus area and is also the general approach taken for these types of estimates [e.g., Fox Maule

### 3. Experimental Design and Methods

We designed two deterministic numerical models using COMSOL Multiphysics (COMSOL, Inc.), an automated partial differential equations solver utilizing finite elements, to test different physical aspects of the hypothesis (Figures 2 and 3 and sections 3.1–3.2 describe and illustrate these models in detail). One is a model to test the effect of groundwater on the thermal structure of the simulated crust and ice sheet in East Antarctica (see Figure 2 and section 3.1). The other model tests the relation of ice sheet evolution and groundwater dynamics (see Figure 3 and section 3.2). Finally, thermal data from various sources for East Antarctica and Australia (formerly connected along a shared tectonic plate margin) were compiled in context along with geophysical data to delineate areas where the models’ results suggest they may be important in present day East Antarctica. All of the parameters we used in the two different numerical models

**Table 1.** Parameters Used in the Two Different Numerical Models With References, if Applicable<sup>a</sup>

Parameter	Value	Units	Parameter Description	Model Usage	References
A	$5 \times 10^{-3}$	$\text{m}^{-1}$	Hydraulic conductivity decay parameter	M, T	Jiang et al. [2009]
b	$5 \times 10^{-3}$	$\text{m}^{-1}$	Porosity decay term	T	Sclater and Christie [1980]; Jiang et al. [2010]
$C_{p,i}$	2093	$\text{J}/(\text{kg} \times \text{K})$	Specific heat capacity, ice	T	Mellor and Kantha [1989]
$C_{p,w}$	4186	$\text{J}/(\text{kg} \times \text{K})$	Specific heat capacity, water	T	
D	10	km	Crustal length scale	T	Jaupart [1986]; Waples [2001]
g	9.81	$\text{m}/\text{s}^2$	Acceleration due to gravity	M	
H	3000	m	Total ice sheet thickness added	T	
$k_0$	$10^{-18}, 10^{-16}, 10^{-14}, 10^{-12}, 10^{-10}$	$\text{m}^2$	Bed surface permeability	M	Singhal and Gupta [2010]; Gleeson et al. [2011, 2014]
L	$3.3 \times 10^5$	J/kg	Latent heat, $\text{H}_2\text{O}$	T	Mellor and Kantha [1989]
m	1.317		Ice accumulation parameter	T	Price et al. [2002]
$Q_0$	0.5, 5.0	$\mu\text{W}/\text{m}^3$	Heat production, surface of basement rock	T	Sandiford and McLaren [2002]; McLaren et al. [2003]
$Q_s$	1.0	$\mu\text{W}/\text{m}^3$	Heat production, sedimentary rock	T	Waples [2001]
S	$1.02 \times 10^{-10}$	$\text{Pa}^{-1}$	Storage coefficient	M	Lemieux et al. [2008b]
$T_b$	580	°C	Temperature, Curie depth	T	Fox Maule et al. [2005]; Rajaram et al. [2009]
$T_i$	-50	°C	Temperature, average ice sheet surface	T	Comiso [2000]; Price et al. [2002]
$T_m$	-2.61	°C	Temperature, ice-bed interface	T	Siegert and Dowdeswell [1996]
$u_{i,0}$	-73	mm/yr	Ice sheet surface ice accumulation rate	T	Mosley-Thompson et al. [1999]; Price et al. [2002]
$V_0$	-10, -1, 0, 1, 10	mm/yr	Sediment surface groundwater volume flux	T	
Z	0.2		Loading efficiency	M	Lemieux et al. [2008b]
$\kappa_b$	3.2	$\text{W}/(\text{m} \times \text{K})$	Thermal conductivity, basement rock	T	Beardmore and Cull [2001]
$\kappa_i$	2	$\text{W}/(\text{m} \times \text{K})$	Thermal conductivity, ice	T	Mellor and Kantha [1989]
$\kappa_s$	2.8	$\text{W}/(\text{m} \times \text{K})$	Thermal conductivity, sedimentary rock	T	Beardmore and Cull [2001]
$\kappa_w$	0.56	$\text{W}/(\text{m} \times \text{K})$	Thermal conductivity, water	T	
M	$8.94 \times 10^{-4}$	$\text{Pa} \times \text{s}$	Viscosity, water	M	
$\rho_i$	910	$\text{kg}/\text{m}^3$	Density, ice	M (implicit), T	Bamber et al. [2001]
$\rho_w$	1000	$\text{kg}/\text{m}^3$	Density, water	M, T	
$\phi_0$	0.2		Sediment surface porosity	T	Gleeson et al. [2011, 2014]

<sup>a</sup>Parameters designated by "T" are used in the hydrothermal model and "M" for those used in the hydromechanical model. Note that the accumulation rate is negative as it is directed downward.

et al., 2005; Petrunin et al., 2013]. The governing equation in this bottom section is a steady state heat diffusion equation

$$0 = \nabla \cdot (\kappa_b \nabla T) + Q_b \quad (1)$$

where  $\nabla \cdot$  is the divergence (used here in one dimension as  $d/dz$ ),  $\kappa_b$  is the thermal conductivity of the basement rock,  $\nabla$  is the gradient (also used here in one dimension as  $d/dz$ ), T is the temperature to be solved, and  $Q_b$  is a source term for the added radiogenic heat production due to the decay of naturally occurring radioactive elements in the rock. The radiogenic heat production,  $Q_b$ , is evaluated as  $Q_b = Q_0 e^{-d/D}$  [Lachenbruch, 1970], where  $Q_0$  is the heat production at the top of the basement rock which is varied between two values,  $d$  is the depth, and  $D$  is a characteristic length scale typical for this kind of setting [Jaupart, 1986; Waples, 2001]. The two crustal values of basement surface heat production were selected as a representation of a lower ( $0.5 \mu\text{W}/\text{m}^3$ ) and higher ( $5 \mu\text{W}/\text{m}^3$ ) value typical of global continental crust and Australian crust, respectively [Sandiford and McLaren, 2002; McLaren et al., 2003]. The reason for the higher number is that the Australian crust across the extensional margin from East Antarctica has a largely elevated average heat production and is considered analogous for interpreting the possibility of East Antarctic crust along with its limited thermal data [Carson et al., 2013].

The middle section of the column (3–0 km below the ice bed) is a porous medium containing sedimentary rock and water that represents a typical sedimentary basin above the basement rock (for the area indicated in Figure 1) and draws from earlier work for its estimated depth [Studinger *et al.*, 2004; Ferraccioli *et al.*, 2009; Jordan *et al.*, 2013; Aitken *et al.*, 2014; Frederick, 2015]. The governing equation used is the steady state heat advection-diffusion equation

$$\rho_w C_{p,w} u_w \cdot \nabla T = \nabla \cdot (\kappa_{eq} \nabla T) + Q_s \quad (2)$$

where  $\rho_w$  is the density of the water in the pore space,  $C_{p,w}$  is the specific heat capacity of the water,  $u_w$  is the groundwater volume flux [Stauffer, 2006],  $\kappa_{eq}$  is the equivalent thermal conductivity of the porous medium and fluid mixture, and  $Q_s$  is the bulk radiogenic heat production of that mixture (only the sediment is radiogenic though). The left hand side of the equation is the convective component and the first term of the right hand side (RHS) is the diffusive component. The volume flux of the water,  $u_w$ , is prescribed as  $u_w = V_0 e^{-Ad}$ , where  $V_0$  is the groundwater volume flux at the top of the sediment column varied in the model from –10 to 10 mm/yr (conservatively low for the vertical component of typical groundwater volume flux magnitudes from topographically driven flow),  $A$  is a decay parameter typical for this kind of setting [Jiang *et al.*, 2009], and  $d$  is the depth. The exponential decay in volume flux magnitude correlates with an exponential decrease in sediment porosity (and permeability) with depth (á la Athy [1930], Sclater and Christie [1980], and McKenna and Sharp [1998]). As we do not treat permafrost formation in this model (to give proper treatment for this would require extensive computational expense), we did not allow the prescribed volume of water to be temperature dependent (i.e., approaching zero as the pressure-melting temperature is reached). The approach is reasonable as studies suggest much of the area under the ice sheet shown in Figure 1 is at the pressure melting temperature [e.g., Siegert and Dowdeswell, 1996; Pattyn, 2010; Van Liefferinge and Pattyn, 2013] and is validated here given that only one of the ten simulations produced a basal temperature below the pressure melting temperature. The equivalent thermal conductivity of the porous medium,  $\kappa_{eq}$ , is evaluated as  $\kappa_{eq} = \phi \kappa_w + (1 - \phi) \kappa_s$ , where  $\kappa_w$  is the thermal conductivity of water,  $\kappa_s$  is a typical sedimentary rock thermal conductivity [Beardsmore and Cull, 2001], and  $\phi$  is the porosity. The porosity,  $\phi$ , is evaluated as  $\phi = \phi_0 e^{-bd}$  [Athy, 1930], where  $\phi_0$  is the surface porosity of a typical crustal value [Gleeson *et al.*, 2011; Gleeson *et al.*, 2014],  $b$  is a porosity decay term appropriate for this kind of setting [Sclater and Christie, 1980; Jiang *et al.*, 2010], and  $d$  is the depth.

The top section (0–3 km above the ice bed) of the model represents a simulated column of ice proximal to an ice sheet divide (see Figure 1 for general area of applicability). The governing equation used is a steady state heat advection-diffusion equation similar to above but lacks a source term and allows for the phase change of ice and water

$$\rho C_p u_i \cdot \nabla T = \nabla \cdot (\kappa \nabla T) \quad (3)$$

where  $\rho$  is the density of the fluid (ice or water; temperature dependent),  $C_p$  is the specific heat capacity of the fluid,  $u_i$  is the vertical advection of the ice, and  $\kappa$  is the thermal conductivity of the fluid. The vertical advection of ice,  $u_i$ , is defined as a depth dependent function  $u_i = u_{i,0} (1 - \frac{H-z}{H})^m$  [Price *et al.*, 2002] where  $u_{i,0}$  is equal to the average surface accumulation rate (negative value here as it is directly downward) of ice typical for interior East Antarctica [Mosley-Thompson *et al.*, 1999; Price *et al.*, 2002],  $H$  is the total thickness of the ice sheet,  $m$  is an accumulation parameter typical for interior East Antarctica [Price *et al.*, 2002], and  $z$  is the elevation from the ice sheet base. The pressure melting temperature for the ice is evaluated as  $T_m = 0^\circ\text{C} - \frac{H}{1149 \text{ [m]}}$  [Siegert and Dowdeswell, 1996] which equates to  $-2.61^\circ\text{C}$  for this model. The density of the fluid,  $\rho$ , is evaluated as  $\rho = \frac{\theta \rho_i C_{p,i} + (1 - \theta) \rho_w C_{p,w}}{\theta C_{p,i} + (1 - \theta) C_{p,w}}$  where  $\theta$  is the fraction of ice,  $\rho_i$  is the density of ice,  $\rho_w$  is the density of water,  $C_{p,i}$  is the specific heat capacity of ice, and  $C_{p,w}$  is the specific heat capacity of water. The specific heat capacity,  $C_p$ , of the material is evaluated as  $C_p = \theta C_{p,i} + (1 - \theta) C_{p,w} + L \frac{d(1-\theta)}{dT}$  where  $L$  is the latent heat from ice melting to water. Note that the latent heat term is not time-dependent and is critical for calculating the steady phase boundary between water and ice in this section of the model domain (initially all ice in the model setup). The thermal conductivity,  $\kappa$ , is evaluated as  $\kappa = \theta \kappa_i + (1 - \theta) \kappa_w$ , where  $\kappa_i$  is the thermal conductivity of ice and  $\kappa_w$  is the thermal conductivity of water. These formulations are based on the module for heat transfer accounting for phase change in COMSOL Multiphysics (v4.3b).

The governing equations (equations (1)–(3)) were solved using COMSOL Multiphysics with a mesh size of 1 m giving 36,000 domain elements. Dirichlet boundary conditions we used in the model are temperature conditions at the top and bottom. A temperature at the bottom,  $T_b$ , of  $580^\circ\text{C}$  represents the Curie isotherm

and the top,  $T_i$ , with  $-50^\circ\text{C}$  for the ice sheet surface. We selected the temperature at the Curie isotherm based on common usage for this depth [Fox Maule *et al.* 2005; Rajaram *et al.* 2009] while the ice sheet surface temperature is an annual average for present day, interior East Antarctica [Comiso, 2000; Price *et al.* 2002]. Due to Comsol's solving efficiency, current notebook computer performance, and the problem's single dimension in steady state, the solution time was within minutes.

### 3.2. Experimental Design and Methods: Hydromechanical Model

To test the effect of potential East Antarctic Ice Sheet evolution on the groundwater volume flux at the ice-bed interface, we created a transient one-dimensional, numerical groundwater model (see Figure 3 for details). The model was largely based on the same approach used by Lemieux *et al.* [2008b] to validate a three-dimensional continental groundwater model forced by ice sheet model output. The domain of the model is a sedimentary basin with fully saturated (i.e., Darcy flow) pore space similar to the basin in the previous model. The ice sheet was evolved through a partial mock glacial cycle that is simulated by growing (advance) and shrinking (retreat) a water equivalent ice column over the top of the 3 km sediment column. While the specific timing used here is arbitrary and the same as used by Lemieux *et al.* [2008b], the rate of change is similar to that of rapidly declining ice elsewhere in Antarctica [Christoffersen *et al.*, 2014]. While this model could have been coupled to the hydrothermal model described in the previous section, the goal with this model was to deterministically simulate solely the transient pressure effects of an ice sheet on a groundwater system given similar geometry and parameters typical of the area of focus in East Antarctica shown in Figure 1. Again, Table 1 contains all of the parameter information we used in the model simulation along with references for usage precedence. This model is governed by a form of the transient groundwater flow equation that is partially coupled to the ice sheet stress (i.e., vertical only) [see Ingebritsen *et al.*, 2006].

$$\rho_w S \frac{\partial P}{\partial t} - \nabla \cdot \rho_w \left( \frac{k}{\mu} \nabla P \right) = \rho_w \zeta \frac{\partial \sigma_{zz}}{\partial t} \quad (4)$$

where  $\rho_w$  is the density of water (representing a density equivalent of ice; see Figure 3),  $S$  is the uniaxial specific storage,  $P$  is the pore water pressure to be solved,  $\nabla \cdot$  is the divergence (used here in one dimension as  $d/dz$ ),  $k$  is the matrix permeability,  $\mu$  is the viscosity of the water,  $\nabla$  is the gradient (also used here in one dimension as  $d/dz$ ),  $\zeta$  is the one-dimensional loading efficiency, and  $\sigma_{zz}$  is the vertical stress from the ice sheet. The right hand side of the equation is an a priori source term that represents the addition of pore pressure from the ice sheet [see Neuzil, 2012]. The loading efficiency is set at 0.2 and the specific storage at  $1.02 \times 10^{-10} \text{ Pa}^{-1}$ , which are consistent with Lemieux *et al.* [2008b]. We evaluate the matrix permeability,  $k$ , using an exponential decay model (unlike Lemieux *et al.* [2008b]) where  $k = k_0 e^{-Ad}$ ; where  $k_0$  is the permeability at the top of the sediment column varied in the model through a wide hydrogeologic range,  $A$  is the same decay parameter as used before [Jiang *et al.*, 2009], and  $d$  is the depth. The surface permeability,  $k_0$ , is varied from  $10^{-10}$  to  $10^{-18} \text{ m}^2$  in order to demonstrate a wide range of geologic materials (generally speaking, unconsolidated sand or gravel to unfractured mudrock or massive crystalline rock). The vertical stress from the ice sheet,  $\sigma_{zz}$ , is evaluated as  $\sigma_{zz} = \rho_w g h(t)$  where  $\rho_w$  is the water density,  $g$  is the acceleration due to gravity, and  $h(t)$  is the water equivalent ice sheet height at a given time. The ice sheet starts out at 0 m at 0 kyr and linearly grows to a maximum added height of 3000 m water equivalent ( $\sim 3300$  m of ice) at 10 kyr. After reaching the peak thickness, the ice sheet linearly shrinks back to 0 m of ice at 20 kyr ending the model simulation, consistent with Lemieux *et al.* [2008b].

As before, we modeled the numerical simulations using COMSOL Multiphysics. The domain of 3 km used a 1 m mesh size for a total of 3000 elements. The governing equation (equation 4) was solved with the Dirichlet boundary condition of a given hydraulic head function,  $h(t)$ , at the top (0 km) and a source term throughout (RHS of equation 4) the domain. The simulation was iterated through a partial mock glacial cycle using each of the given values of surface permeability ( $k_0$ ). We used a 500 year time step in order to balance accuracy, solution time, and output data size. Again, due to Comsol's solving efficiency, current notebook computer performance, and the problem's single dimension with time dependence the solution time was within minutes.

### 3.3. Experimental Design and Methods: East Antarctic Areas of Higher Heat Potential and Groundwater Impact

In order to relate the previous method's results to a real-world setting of great societal interest (i.e., sea level rise component from the marine-grounded East Antarctic Ice Sheet), we created a subglacial map detailing

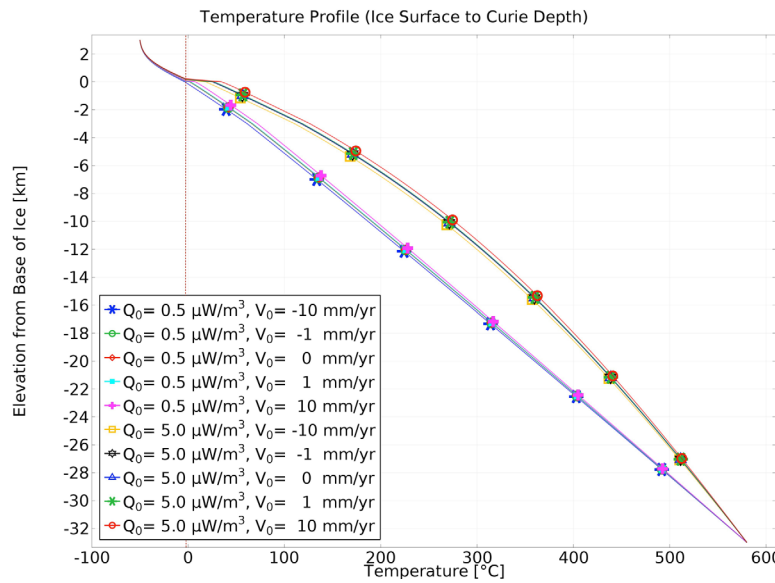


**Figure 4.** Temperature profile with depth from the steady state 1-D hydrothermal model results. The model extends from ice sheet surface (3 km) through the sedimentary basin and crystalline basement (~3 km) to the base of the magnetic crust, or Curie depth (~33 km). Base-  
ment surface radiogenic heat production,  $Q_0$ , and sediment surface groundwater volume flux,  $V_0$ , parameters are plotted. Note that the  
dominant factor in the two temperature groups in the deeper subsurface is the radiogenic heat production value. The dashed red line is  
meant to assist the reader in quickly identifying the pressure melting temperature of ice at the ice-bed interface and does not represent  
the pressure melting temperature in the subsurface of Earth.

areas where the above experiments' results may be most likely influential to ice sheet dynamics. We created this map by using current crustal thermal data, tectonic plate reconstruction, and geophysically derived geologic maps from publicly available data. Some of the surface radiogenic heat production data in Australia come from the publically available Global Heat Flow Database (<http://www.heatflow.und.edu/>). The heat production data in East Antarctica are from *Carson and Pittard* [2012]. We calculated the bulk of the present-day heat production data from the Australian OZCHEM surface geochemistry database [*Champion et al.*, 2007] using the same method as *Carson and Pittard* [2012] used which is based on *Turcotte and Schubert* [2002]. The tectonic interpretations across East Antarctica and Australia from *Aitken et al.* [2014] serve as a rough guide to tectonic province delineation in the East Antarctic. Aerogeophysical surveys from the University of Texas Institute for Geophysics and other collaborations [e.g., *Young et al.*, 2011; *Frederick*, 2015] are principally over the Wilkes and the Aurora Subglacial Basins of East Antarctica. These surveys comprise gravimetric and ice-penetrating radar data sets among others, which we used to define sedimentary basin depth and extent. Gravity data are useful in delimiting less dense sedimentary basins and their depths from the surrounding, denser crystalline basement rock. Ice-penetrating radar data are useful not only for imaging internal ice sheet structure and ice bottom depth (Bedmap2 used) [*Fretwell et al.* [2013] but also in mapping out bed roughness [*Shepherd et al.*, 2001]. The bed roughness (root mean squared deviation of detrended bed elevation data on a 1600 m baseline) we used here to define extents of smoother (i.e., low roughness) sedimentary terrains interpreted as softer sedimentary land surfaces or previously shallow marine settings. We constructed a somewhat conservative and arbitrary approach to citing zones of higher probable groundwater impact (see Figure 8) to ice sheet dynamics by selecting only the zones of overlap of relatively low bed roughness (cutoff height of about 20 m) and areas of at least 1 km of gravity-derived sediment thickness (for higher confidence in delineation). This approach ensured that potential basin-to-regional-scale groundwater flow systems could be delineated in a relatively conservative approach, relying on the combination of two independent geophysical constraints (i.e., electromagnetic and gravimetric). We used ArcGIS (ESRI, v10.2) and PaleoGIS (The Rothwell Group, L.P., v4.2), a tectonic plate reconstruction software, to interpret all of the data together. We used a plate reconstruction model to connect East Antarctica and Australia at 160 Ma, in keeping with *Aitken et al.* [2014]. Once the East Antarctic and Australian plates were reconnected, we calculated basic statistical functions (average, standard deviation, etc.) for each of the heat production groupings (see Figure 8 for the selected rectangular regions) delineated by data point proximity and correlation to roughly defined tectonic provenances [*Carson et al.*, 2013; *Aitken et al.*, 2014].

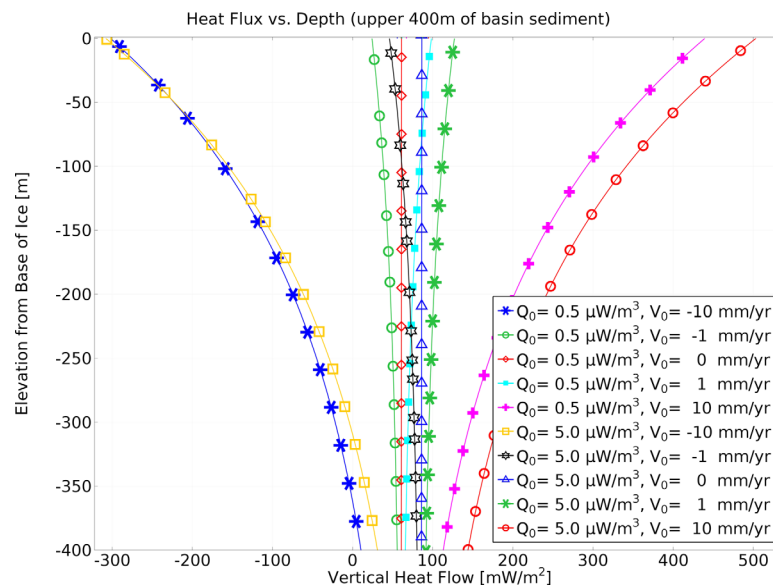


**Figure 5.** Vertical heat flux in the upper 400 m of the sedimentary basin (0 to  $-0.4$  km) from the steady state 1-D hydrothermal model results. Basement surface radiogenic heat production,  $Q_0$ , and sediment surface groundwater volume flux,  $V_0$ , parameters are plotted. Radiogenic heat production in the sedimentary rock (down to 1 km from the base of the ice) is uniformly  $1 \mu\text{W}/\text{m}^3$  throughout. Positive  $V_0$  is a volume flux moving in the upward direction. Greater heat flux mostly occurs when the water volume flux is positive but heat production is also an important factor.

## 4. Results

### 4.1. Results: Hydrothermal Model

One of the main trends in the hydrothermal model results is the grouping in temperature profiles (see Figure 4). As expected in the sediments and basement rock, the temperature profiles with the higher heat production ( $5 \mu\text{W}/\text{m}^3$ ) curve upward from the linear trend expected had no heat production been added. The profiles with the lower heat production ( $0.5 \mu\text{W}/\text{m}^3$ ) group closer to that linear trend. The modeled temperatures in the ice sheet are nearly identical for much of the ice column. The temperature profiles for all of the results are equal at the model domain top and bottom (i.e., boundary conditions). A major slope break occurs at the ice-bed interface (at 0 km). In all but one ( $Q_0 = 0.5 \mu\text{W}/\text{m}^3$  and  $V_0 = -10 \text{ mm/yr}$ ) of the resulting temperature profiles, the ice is above the pressure melting temperature of  $-2.6^\circ\text{C}$  (see zoom of Figure 4 in supporting information Figure S4). The simulated temperatures at the ice-bed interface range from about  $-4$  to  $35^\circ\text{C}$ . The resulting phase change in all but one of the profiles results in the conversion of ice to water in the column. This essentially simulates a one-dimensional subglacial lake under an ice sheet where the bottom of the column is liquid water and the ice sheet is above it. The columns of basal water range in height from 32 to 220 m (see supporting information Figure S5 for phase change plot).

Another prominent trend in the model results is the simulated vertical heat flux in the uppermost portion of the sedimentary basin (see Figure 5) where the groundwater volume flux is the dominant factor in heat advection. The highest positive vertical heat flux values (peak of  $\sim 440\text{--}500 \text{ mW/m}^2$  at 0 km elevation) correlate to the model runs using the highest positive groundwater volume fluxes (max of  $10 \text{ mm/yr}$ ). Likewise, the most negative vertical heat flux (peak of  $\sim -300 \text{ mW/m}^2$  at 0 km elevation) correlates to where the heat flux is advected via groundwater downward at a max of  $-10 \text{ mm/yr}$  at 0 km elevation. The values clustering in the middle of Figure 5 ( $V_0 = -1$  to  $1 \text{ mm/yr}$ ) span a range of about  $25\text{--}125 \text{ mW/m}^2$ . Within these, the simulated vertical heat flux values without fluid advection (i.e., volume flux =  $0 \text{ mm/yr}$ ) are at roughly  $60$  and  $85 \text{ mW/m}^2$  (for  $Q_0 = 0.5$  and  $5.0 \mu\text{W}/\text{m}^3$ , respectively). Also within that same cluster, it is observed that a change of  $\pm 1 \text{ mm/yr}$  will alter the vertical heat flux at the ice-bed interface surface by about  $40 \text{ mW/m}^2$ . Another trend in the middle clustering is that, all other things being equal, the difference in heat production choice (i.e.,  $Q_0$ ) results in about a  $20\text{--}25 \text{ mW/m}^2$  difference in simulated heat flux output. The decrease in heat flux with depth is due to the exponential decrease in groundwater volume flux prescribed in the model setup, which is meant to more closely simulate assumed natural conditions.

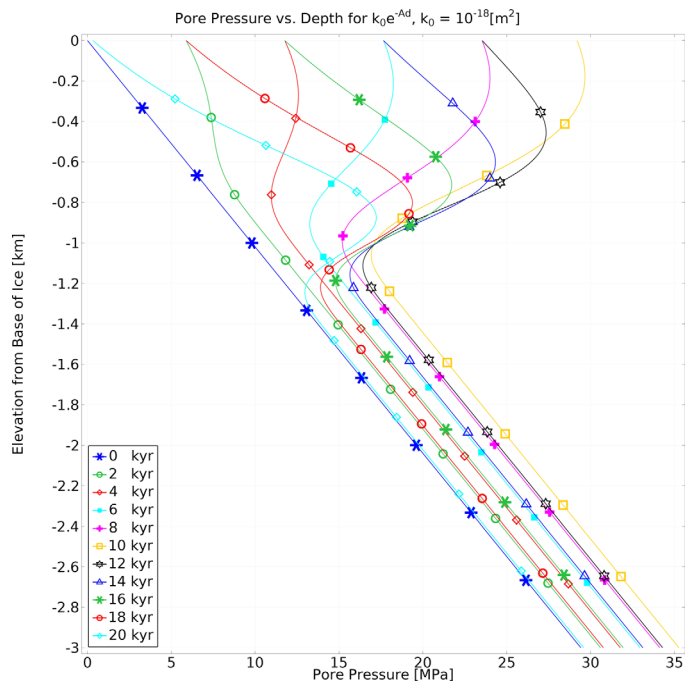


**Figure 6.** Simulated subsurface pore pressure over the partial mock glacial cycle from the transient 1-D hydromechanical model results. The parameterization of permeability,  $k$ , relies on the function  $k = k_0 e^{-Ad}$  where  $k_0$  is equal to  $10^{-18} \text{ m}^2$  in this case (see section 3.2). The plot shows the increase in shallow subsurface pore pressure during ice advance and the anomalous, or fossil, pore pressure as the ice retreats.

Pore pressure can be converted to hydraulic head; a converted plot of Figure 6 is included in supporting information Figure S8.

The main behavior of the simulated pore pressure is that the addition of the growing ice overburden pressure adds to the top of the domain unevenly until the ice sheet shrinks leaving the pressure at the top lower than that part of the way down. This disequilibrium of pressure causes higher pore pressure in the subsurface leading to volume fluxes of water infiltrating into (recharge) or exfiltrating out of (discharge) the surface of the sediment (ice-bed interface). Figure 7 shows this behavior in detail for each parameterization. At the beginning (0 kyr) all of the parameterizations are essentially (with some numerical error) at zero volume flux but as the simulation time advances they quickly differ. The highest surface permeability parameters ( $10^{-10}$  and  $10^{-12} \text{ m}^2$ ) quickly reach a maximum input of about  $-0.72 \text{ mm/yr}$  almost instantaneously whereas the rest are more or less evenly spread out (differing by about  $0.2 \text{ mm/yr}$ ). As the ice sheet pressure adjusts, the parameterizations act largely (again, with some numerical error) symmetrical to the ice advance pattern. As before, the highest surface permeability parameters quickly reach a maximum output of about  $0.72 \text{ mm/yr}$  almost instantaneously whereas the rest are more or less evenly spread out through 20 kyr. The magnitude of volume flux for the rest of the surface permeability parameters vary from 0.2 to  $0.6 \text{ mm/yr}$ . Given added simulation time past 20 kyr (not shown in Figure 7), it can take an additional few hundred to tens of thousands of years, depending on the parameterization, for the surface exchange to return to the initial condition (i.e., 0 mm/yr).

#### 4.3. Results: East Antarctic Areas of Higher Heat Potential and Groundwater Impact

The mapping of the extents of this research's relevant impact to under the East Antarctic Ice Sheet is shown entirely in Figure 8. Our effort produced a map of the regions where groundwater flow systems may possibly be extent at the basin-to-regional scale in East Antarctica. The map is also a first attempt at trying to roughly estimate the degree of heterogeneity in the near-surface thermal properties of the East Antarctic crust by extension of known values in the previously connected continent of Australia ( $\sim 160 \text{ Ma}$ ) via geochemical interpretation, along with some limited geochemical data from East Antarctica. The groupings of surface heat production largely cluster into the three provinces of heat flow in Australia (see the rectangular

#### 4.2. Results: Hydromechanical Model

The main outputs for the hydromechanical model are subsurface pore pressure and the surface exchange, which is the groundwater volume flux at the surface (i.e., top) of the one-dimensional model. The simulated pore pressures shown in Figure 6 demonstrate the subsurface behavior through a portion of a mock glacial cycle (20 kyr here as in Lemieux et al. [2008b]) for one of the parameterizations of surface permeability ( $k_0 = 10^{-18} \text{ m}^2$ ). The fossil, or anomalous, pore pressure is observed as bulges of increasing pressure down to about 1.2 km in depth, which relates to the exponential drop in permeability with depth. All but one ( $k_0 = 10^{-10} \text{ m}^2$ ) of the parameterizations modeled exhibit similar behavior to the one shown in Figure 6 but with slightly less exaggeration of fossil pore pressure and are not included.

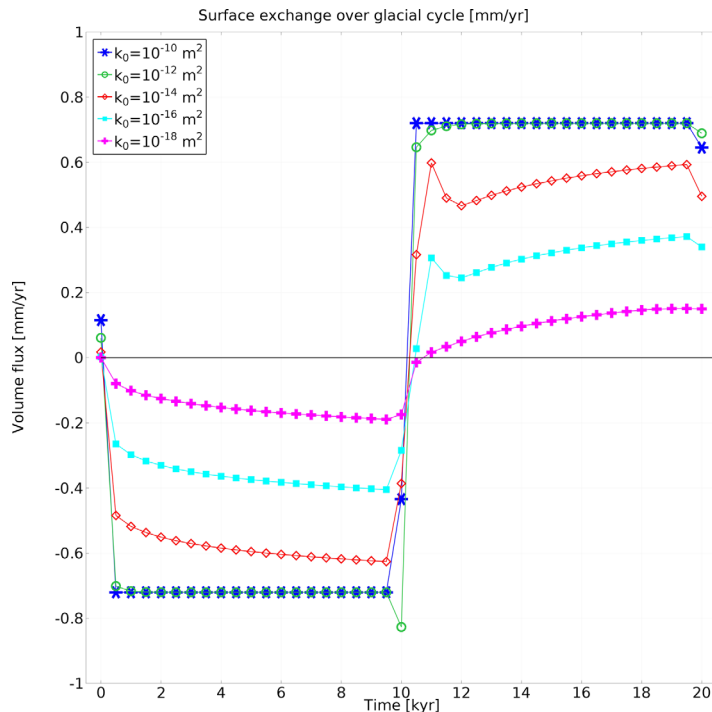


**Figure 7.** Vertical water volume flux (exchange flux) at the ice-bed interface over a simplified partial glacial cycle from the transient 1-D hydromechanical model. Positive flux is upward out of the sediment surface (i.e., discharge or exfiltration). The ice sheet steadily advances leading to a maximum at 10 kyr with steady retreat following. Subsurface recharge (or infiltration) occurs during ice advance and discharge occurs with retreat. The parameterization of permeability,  $k$ , relies on the function  $k = k_0 e^{-Ad}$  (see section 3.2).

*Aitken et al.* [2014] and are a part of the South Australian heat flow anomaly [see *Sandiford and McLaren*, 2002; *McLaren et al.*, 2003; *Carson et al.*, 2013]. The values in Group C largely come from a different and varied cratonic history than those in Group A and are much younger in age on average. The areas which groundwater may have some impact on ice sheet dynamics and water budgets (see section 3.3) are mostly located distal to the coastline of East Antarctica with the exception of some large, coastal outlet glacier areas containing deep sedimentary valleys. The bulk of the areas of probable groundwater impact are largely in areas presently at or below present-day sea level (lying mostly within extents of the Aurora and Wilkes subglacial basins; see Figure 8). The largest groundwater impact areas' longest axes (specifically in the Wilkes and Aurora subglacial basins) tend to coincide with the longer tectonic interpretations of *Aitken et al.* [2014].

## 5. Discussion

The one-dimensional hydrothermal model, while a highly simplified version of reality, demonstrates the basic but important impact the advection of heat flux via groundwater can contribute when added to diffusive heat flux (shown here by adding as much as 380–415 mW/m<sup>2</sup>). The values with diffusion alone (roughly 60 and 85 mW/m<sup>2</sup>) are consistent with those estimated by *Fox Maule et al.* [2005] with the lower value also consistent with those of *Shapiro and Ritzwoller* [2004] in East Antarctica. One main simplification inherent with one-dimensional modeling is the absence of horizontal effects, in particular here, as horizontal heat flux by groundwater or ice sheet flow. This effect has been studied by *Waddington* [1987] and shown to be important. Future work should include this when extending this approach to multidimensional models. Although the simulated lake depths represent equilibrium levels (the model is unable to drain water from under the ice column), the range of lake depths (32–220 m) for all but one of the simulations (one had ice frozen to the bed) is consistent with those observed (see current inventory from *Wright and Siegert* [2012]). The results from the hydrothermal model demonstrate that even with moderately low groundwater volume flux magnitudes, the vertical heat flux magnitude under the interior of the East Antarctic Ice Sheet can be

boxes A–C in Figure 8 and *McLaren et al.* [2003]). The average heat production in Group A is 1.08  $\mu\text{W}/\text{m}^3$  with a standard deviation of 1.53  $\mu\text{W}/\text{m}^3$ . The statistical calculations for Group A used 2044 data points from Australia and 55 data points from East Antarctica. The average heat production in Group B is 4.27  $\mu\text{W}/\text{m}^3$  with a standard deviation of 28.75  $\mu\text{W}/\text{m}^3$ . The statistical calculations for Group B used 2132 data points from Australia and 34 data points from East Antarctica. The average heat production in Group C is 1.43  $\mu\text{W}/\text{m}^3$  with a standard deviation of 2.59  $\mu\text{W}/\text{m}^3$ . The statistical calculations for Group C used 9702 data points from Australia and 224 data points from East Antarctica. Group B represents the Mawson/Gawler cratonic connection [*Carson et al.*, 2013; *Aitken et al.*, 2014] with the values of heat production being tightly connected to the tectonic interpretations of

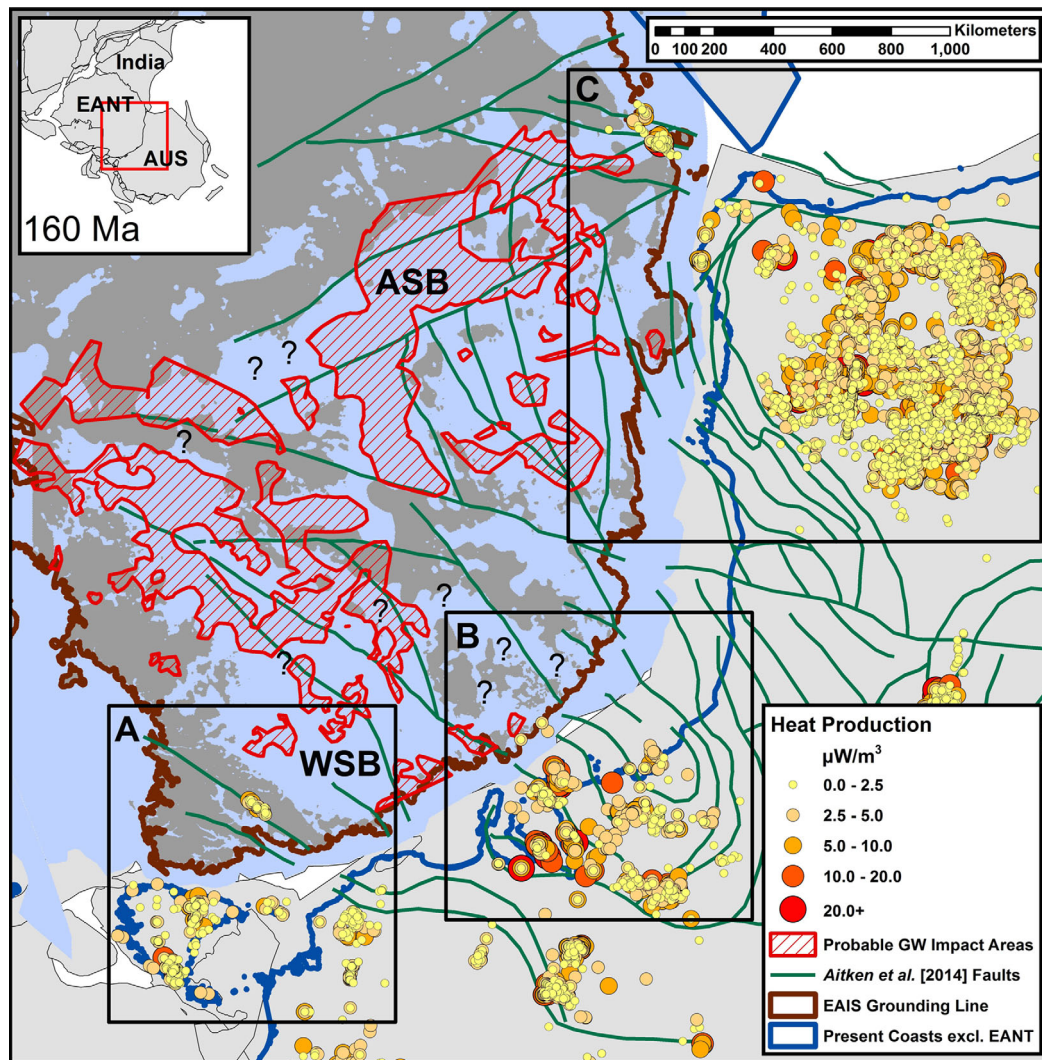


**Figure 8.** Map of the reconstructed assemblage of the East Antarctic (EANT) and Australian (AUS) plates at 160 Ma with present day, surface radiogenic heat production values (calculated mainly from Champion *et al.* [2007] and Carson and Pittard [2012]). The relative global tectonic plate (plates in light gray) assemblage at 160 Ma and the extent of the study area are shown in the inset map. The grouping extents used for the heat production statistics are in each of the lettered boxes. The averages for the heat production groupings are 1.08 (standard deviation 1.53), 4.27 (std. 28.75), and 1.43 (std. 2.59)  $\mu\text{W}/\text{m}^3$  for boxes A, B, and C, respectively. The geophysically derived fault and tectonic interpretations from Aitken *et al.* [2014] are shown with green lines. The Wilkes Subglacial Basin (WSB) covers much of the area at or below sea level from the coast toward the South Pole. The Aurora Subglacial Basin (ASB) extends in a similar manner to the WSB but from a different direction; it also terminates near the WSB's terminus. Probable groundwater impact areas (see section 3.3) are included as red-hatched zones. Areas where the present-day bed elevation from Fretwell *et al.* [2013] is at or below mean sea level are colored blue and those above are in dark gray. Locations where geophysical data availability is limited or nonexistent and are of added hydrogeological and geochemical interest in line with this study for future aerogeophysical surveying are designated with question marks (?). The present-day East Antarctic Ice Sheet (EAIS) grounding line from Bohlander and Scambos [2007] is included in brown. Present-day coastlines [Wessel and Smith, 1996; v2.3.3] on other plates are shown as blue lines.

modified dramatically. This added complexity to the geothermal heat flux parameterization for continental ice sheet models could add significant value to their usage if incorporated.

The one-dimensional hydromechanical model, while also a highly simplified version of reality, demonstrates how changes in ice sheet thickness not only alter the pressure potential of the subglacial water and groundwater but also how the timing of the change can result in unsteady subsurface pore pressures. This disequilibrium in pore pressure causes groundwater to infiltrate into the saturated sediment during ice sheet thickening and exfiltration upon ice thinning similarly observed by Lemieux *et al.* [2008b]. The magnitude of the rates of surface groundwater volume flux can reach 0.6–0.72 mm/yr which given knowledge of the previous model's results would equate to about a 24–28.8  $\text{mW}/\text{m}^2$  change in the heat flux magnitude. This

significant alteration to the geothermal heat flux could occur at discrete locations (i.e., fault zones) or across widespread areas in the sedimentary basins underneath the East Antarctic Ice Sheet. The groundwater volume fluxes simulated here are only a fraction of those estimated by Christoffersen *et al.* [2014], which are up to roughly one order of magnitude greater, for the marine-grounded Siple Coast ice streams in West Antarctica. Currently, in much of the East Antarctic the ice sheet is generally not as dynamic as in West Antarctica although, as recent work indicates, East Antarctica experienced great changes when compared to present day activity not long ago in the geologic record [Mackintosh *et al.*, 2011; Young *et al.*, 2011; Mengel and Levermann 2014; Pollard *et al.*, 2015].

We sought to roughly outline the extent of probable areas where groundwater could potentially act similar to the model simulations and also roughly map the heterogeneity of surface heat production in East Antarctica in Figure 8. The resulting figure conservatively estimates that areas shown to have probable groundwater flow systems exist in mostly submarine areas under the East Antarctic Ice Sheet. This area is more prone to ice sheet change from climatic forcing [Young *et al.*, 2011; Pollard *et al.*, 2015] which increases the significance of groundwater as a subglacial process there. The fact that these sedimentary basin surfaces are generally lower than their surrounding topography is not surprising but as this terrain becomes overlain by ice they are both dramatically lowered (albeit unequally due to erosional and isostatic differentials) with deeper depressions existing more inland under the thicker ice. The probable groundwater impact areas locations are significantly inland and are most likely due to this effect and the long, complicated geologic history of the intracratonic sedimentary basins of East Antarctica. The heat production data statistics demonstrate the heterogeneity of the geologic surface across the East Antarctic-Australian continental margin. The data, coupled with our model results, suggest that higher, heterogeneous geothermal heat fluxes are more likely throughout East Antarctica than previously estimated [e.g., Shapiro and Ritzwoller, 2004; Fox Maule *et al.*, 2005; Pollard *et al.*, 2005], especially in areas where groundwater flow systems are potentially present. While this may not be greatly significant by itself, our initial attempt to estimate the areas over which these specific processes could potentially play a role in ice sheet dynamics coupled to the deterministic model results could be very significant.

## 6. Conclusions

The continental ice sheet modeling community will eventually need to incorporate the effects demonstrated here when simulating ice dynamics in the interior of the East Antarctic Ice Sheet if higher accuracy estimates of future ice volume are to be calculated. While it is highly likely that the physical effects presented here are not as crucial to understand in areas of higher ice velocity (i.e., outlet glaciers), a significant fraction of the total ice sheet maybe affected by such processes and, thus, should be considered. For example, the added complexity to the geothermal heat flux parameterization for continental ice sheet models could add significant value to their usage if incorporated. Further efforts to better define the subglacial geology of the region will help resolve the great uncertainties that exist in the thermal and mechanical properties of the East Antarctic subsurface and lead to better estimations of heat flux and groundwater volume flux rates (specifically targeting the areas denoted in Figure 8 as question marks). Future efforts in continuing to test the aforementioned hypothesis should focus on coupling these processes together in multidimensional models. This work should also eventually couple these physical processes to the flow of water at the ice-bed interface, as well as, to the flow of the ice sheet above in order to gain an overall better understanding of this poorly understood, critically important natural system.

## Acknowledgments

Supporting Information figures can be found at online version of this article. We thank L. Wang, K. Befus, M. Hesse, and B. Cardenas for their assistance with Comsol Multiphysics. For assistance with Matlab for data analysis, we thank C. Greene; and for PaleoGIS, we thank J. Davis. We thank B. Frederick for assistance with and usage of his finalized geophysical estimations of sedimentary basin thickness in East Antarctica. Finally, we thank K. Soderlund, Y. Yokoyama and two anonymous reviewers for their constructive feedback. Funding to support this work was provided by the G. Unger Vetlesen Foundation, OPP 99-11617 and NNX08AN68G, as well as, the UTIG Gale White Fellowship supporting the lead author. This is UTIG contribution 2947.

## References

- Aitken, A. R. A., D. A. Young, F. Ferraccioli, P. G. Betts, J. S. Greenbaum, T. G. Richter, J. L. Roberts, D. D. B., and M. J. Siegert (2014), The subglacial geology of Wilkes Land, East Antarctica, *Geophys. Res. Lett.*, 41, 2390–2400, doi:10.1002/2014GL059405.
- Alley, R. B. (1989), Water-pressure coupling of sliding and bed deformation: I. Water system, *J. Glaciol.*, 35(119), 108–118.
- Athy, L. F. (1930), Density, porosity, and compaction of sedimentary rocks, *AAPG Bull.*, 14(1), 1–24.
- Bamber, J. L., R. L. Layberry, and S. P. Gogineni (2001), A new ice thickness and bed data set for the Greenland ice sheet: 1. Measurement, data reduction, and errors, *J. Geophys. Res.*, 106(D24), 33,773–33,780.
- Beardmore, G. R., and J. P. Cull (2001), *Crustal Heat Flow: A Guide to Measurement and Modelling*, 324 pp., Cambridge Univ. Press, Cambridge.
- Bense, V. F., and M. A. Person (2008), Transient hydrodynamics within intercratonic sedimentary basins during glacial cycles, *J. Geophys. Res.*, 113, F04005, doi:10.1029/2007JF000969.
- Bindschadler, R., H. Choi, and ASAID Collaborators (2011), *High-resolution Image-derived Grounding and Hydrostatic Lines for the Antarctic Ice Sheet*, Natl. Snow and Ice Data Cent., Boulder, Colo., doi:10.7265/N56T0JK2.

- Blankenship, D. D., C. R. Bentley, S. T. Rooney, and R. B. Alley (1986), Seismic measurements reveal a saturated porous layer beneath an active Antarctic ice stream, *Nature*, 322, 54–57.
- Blankenship, D. D., R. E. Bell, S. M. Hodge, J. M. Brozena, J. C. Behrendt, and C. A. Finn (1993), Active volcanism beneath the West Antarctic ice sheet and implications for ice-sheet stability, *Nature*, 361, 526–529.
- Blankenship, D. D., D. L. Morse, C. A. Finn, R. E. Bell, M. E. Peters, S. D. Kempf, S. M. Hodge, M. Studinger, J. C. Behrendt, and J. M. Brozena (2001), Geologic controls on the initiation of rapid basal motion for west Antarctic ice streams: A geophysical perspective including new airborne radar sounding and laser altimetry results, in *The West Antarctic Ice Sheet: Behavior and Environment*, edited by R. B. Alley and R. A. Bindschadler, AGU, Washington, D. C.
- Bohlander, J., and T. Scambos (2007), *Antarctic Coastlines and Grounding Line Derived from MODIS Mosaic of Antarctica (MOA)*, Natl. Snow and Ice Data Cent., Boulder, Colo.
- Boulton, G. (2010), Drainage pathways beneath ice sheets and their implications for ice sheet form and flow: The example of the British Ice Sheet during the Last Glacial Maximum, *J. Quat. Sci.*, 25, 483–500.
- Carson, C. J., and M. Pittard (2012), *A Reconnaissance Crustal Heat Production Assessment of the Australian Antarctic Territory (AAT)*, Geoscience Australia Record 2012/63, Geoscience Australia, Canberra, Australia.
- Carson, C. J., S. McLaren, J. L. Roberts, S. D. Boger, and D. D. Blankenship (2013), Hot rocks in a cold place: High sub-glacial heat flow in East Antarctica, *Q. J. Geol. Soc. London*, 171(1), 9–12.
- Champion, D. C., A. R. Budd, M. S. Hazell, and A. Sedgmen (2007), *OZCHEM National Whole Rock Geochemistry Dataset*, Geoscience Australia, Canberra, Australia.
- Christoffersen, P., M. Bougamont, S. P. Carter, H. A. Fricker, and S. Tulaczyk (2014), Significant groundwater contribution to Antarctic ice streams hydrologic budget, *Geophys. Res. Lett.*, 41, 2003–2010, doi:10.1002/2014GL059250.
- Clarke, G. K. C., S. G. Collins, and D. E. Thompson (1984), Flow, thermal structure, and subglacial conditions of a surge-type glacier, *Can. J. Earth Sci.*, 21, 232–240.
- Comiso, J. C. (2000), Variability and trends in Antarctic surface temperatures from in situ and satellite infrared measurements, *J. Clim.*, 13(10), 1674–1696.
- Cutler, P. M., D. R. MacAyeal, D. M. Mickelson, B. R. Parizek, and P. M. Colgan (2000), A numerical investigation of ice-lobe-permafrost interaction around the southern Laurentide ice sheet, *J. Glaciol.*, 46(153), 311–325.
- Drewry, D. (1976), Sedimentary basins of the East Antarctic craton from geophysical evidence, *Tectonophysics*, 36(1), 301–314.
- Echelmeyer, K. (1987), Anomalous heat flow and temperatures associated with subglacial water flow, The Physical Basis of Ice Sheet Modeling, in *Proceedings of the Vancouver Symposium*, August 1987, IAHS Publ., 170, 93–104.
- Ferraccioli, F., E. Armadillo, T. Jordan, E. Bozzo, and H. Corr (2009), Aeromagnetic exploration over the East Antarctic Ice Sheet: A new view of the Wilkes Subglacial Basin, *Tectonophysics*, 478(1–2), 62–77.
- Flowers, G. E., S. J. Marshall, H. Björnsson, and G. K. C. Clarke (2005), Sensitivity of Vatnajökull ice cap hydrology and dynamics to climate warming over the next 2 centuries, *J. Geophys. Res.*, 110, F02011, doi:10.1029/2004JF000200.
- Fox Maule, C., M. E. Purucker, N. Olsen, and K. Mosegaard (2005), Heat flux anomalies in Antarctica revealed by satellite magnetic data, *Science*, 309(5733), 464–467.
- Frederick, B. C. (2015), Submarine sedimentary basin analyses for the Aurora and Wilkes subglacial basins and the Sabrina coast continental shelf, East Antarctica, PhD dissertation, Univ. of Texas, Austin.
- Fretwell, P., et al. (2013), Bedmap2: Improved ice bed, surface and thickness datasets for Antarctica, *Cryosphere*, 7(1), 375–393.
- Gleeson, T., L. Smith, N. Moosdorf, J. Hartmann, H. H. Dürr, A. H. Manning, L. P. H. van Beek, and A. M. Jellinek (2011), Mapping permeability over the surface of the Earth, *Geophys. Res. Lett.*, 38, L02401, doi:10.1029/2010GL045565.
- Gleeson, T., N. Moosdorf, J. Hartmann, and L. P. H. van Beek (2014), A glimpse beneath earth's surface: GLobal HYdrogeology MaPS (GLHYMPS) of permeability and porosity, *Geophys. Res. Lett.*, 41, 3891–3898, doi:10.1002/2014GL059856.
- Grasby, S., K. Osadet, R. Betcher, and F. Render (2000), Reversal of the regional-scale flow system of the Williston basin in response to Pleistocene glaciation, *Geology*, 28(1986), 635–638.
- Grasby, S. E., and Z. Chen (2005), Subglacial recharge into the western Canada sedimentary basin—Impact of Pleistocene glaciation on basin hydrodynamics, *Geol. Soc. Am. Bull.*, 117(3/4), 500–514.
- Hughes, T., A. Sargent, and J. Fastook (2011), Ice-bed coupling beneath and beyond ice streams: Byrd Glacier, Antarctica, *J. Geophys. Res.*, 116, F03005, doi:10.1029/2010JF001896.
- Huybrechts, P., and J. Oerlemans (1988), Evolution of the East Antarctic ice sheet: A numerical study of thermo-mechanical response patterns with changing climate, *Ann. Glaciol.*, 11, 52–59.
- Ingebritsen, S. E., C. E. Neuzil, and W. E. Sanford (2006), *Groundwater in Geologic Processes*, 341 pp., Cambridge Univ. Press, N. Y.
- Jaupart, C. (1986), On the average amount and vertical distribution of radioactivity in the continental crust, in *Thermal Modeling in Sedimentary Basins*, edited by J. Burrus, pp. 33–47, Editions Technip, Paris.
- Jiang, X. W., L. Wan, X. S. Wang, S. Ge, and J. Liu (2009), Effect of exponential decay in hydraulic conductivity with depth on regional groundwater flow, *Geophys. Res. Lett.*, 36, L24402, doi:10.1029/2009GL041251.
- Jiang, X. W., L. Wan, M. B. Cardenas, S. Ge, and X. S. Wang (2010), Simultaneous rejuvenation and aging of groundwater in basins due to depth-decaying hydraulic conductivity and porosity, *Geophys. Res. Lett.*, 37, L05403, doi:10.1029/2010GL042387.
- Jordan, T. A., F. Ferraccioli, E. Armadillo, and E. Bozzo (2013), Crustal architecture of the Wilkes Subglacial Basin in East Antarctica, As revealed from airborne gravity data, *Tectonophysics*, 585, 196–206.
- Lachenbruch, A. H. (1970), Crustal temperature and heat production: Implications of the linear heat-flow relation, *J. Geophys. Res.*, 75(17), 3291–3300.
- Lemieux, J. M., E. A. Sudicky, W. R. Peltier, and L. Tarasov (2008a), Dynamics of groundwater recharge and seepage over the Canadian landscape during the Wisconsinian glaciation, *J. Geophys. Res.*, 113, F01011, doi:10.1029/2007JF000838.
- Lemieux, J. M., E. A. Sudicky, W. R. Peltier, and L. Tarasov (2008b), Simulating the impact of glaciations on continental groundwater flow systems: 1. Relevant processes and model formulation, *J. Geophys. Res.*, 113, F03017, doi:10.1029/2007JF000928.
- Lowe, A. L., and J. B. Anderson (2003), Evidence for abundant subglacial meltwater beneath the paleo-ice sheet in Pine Island Bay, Antarctica, *J. Glaciol.*, 49(164), 125–138.
- Mackintosh, A. et al. (2011), Retreat of the East Antarctic ice sheet during the last glacial termination, *Nat. Geosci.*, 4(3), 195–202.
- McIntosh, J. C., G. Garven, and J. S. Hanor (2011), Impacts of Pleistocene glaciation on large-scale groundwater flow and salinity in the Michigan Basin, *Geofluids*, 11(1), 18–33.
- McKenna, T. E., and J. M. Sharp Jr. (1998), Radiogenic heat production in sedimentary rocks of the gulf of Mexico basin, south Texas, *AAPG Bull.*, 82, 484–496.

- McLaren, S., M. Sandiford, M. Hand, N. Neumann, L. Wyborn, and I. Bastrakova (2003), The hot southern continent; heat flow and heat production in Australian Proterozoic terranes, *Spec. Pap. Geol. Soc. Am.*, 372, 157–167.
- Mellor, G. L., and L. Kantha (1989), An ice-ocean coupled model, *J. Geophys. Res.*, 94(89), 10,937–10,954.
- Mengel, M., and A. Levermann (2014), Ice plug prevents irreversible discharge from East Antarctica, *Nat. Clim. Change*, 4, 451–455.
- Mosley-Thompson, E., J. F. Paskievitch, A. J. Gow, and L. G. Thompson (1999), Late 20th century increase in south pole snow accumulation, *J. Geophys. Res.*, 104(D4), 3877–3886.
- Neuzil, C. E. (2012), Hydromechanical effects of continental glaciation on groundwater systems, *Geofluids*, 12(1), 22–37.
- Neuzil, C. E. (2015), Interpreting fluid pressure anomalies in shallow intraplate argillaceous formations, *Geophys. Res. Lett.*, 42, 4801–4808, doi:10.1002/2015GL064140.
- Pattyn, F. (2008), Investigating the stability of subglacial lakes with a full Stokes ice-sheet model, *J. Glaciol.*, 54(185), 353–361.
- Pattyn, F. (2010), Antarctic subglacial conditions inferred from a hybrid ice sheet/ice stream model, *Earth Planet. Sci. Lett.*, 295(3–4), 451–461.
- Person, M., J. McIntosh, V. Bense, and V. H. Remenda (2007), Pleistocene hydrology of North America: The role of ice sheets in reorganizing groundwater flow systems, *Rev. Geophys.*, 45, RG3007, doi:10.1029/2006RG000206.
- Person, M., V. Bense, D. Cohen, and A. Banerjee (2012), Models of ice-sheet hydrogeologic interactions: A review, *Geofluids*, 12(1), 58–78.
- Petrushin, A. G., I. Rogozhina, A. P. M. Vaughan, I. T. Kukkonen, M. K. Kaban, I. Koulakov, and M. Thomas (2013), Heat flux variations beneath central Greenland's ice due to anomalously thin lithosphere, *Nat. Geosci.*, 6, 746–750, doi:10.1038/ngeo1898.
- Piotrowski, J. (2006), Groundwater under ice sheets and glaciers, in *Glacier Science Environmental Change*, edited by P. G. Knight, pp. 50–60, Blackwell, Malden, Mass.
- Piotrowski, J. A., P. Hermanowski, and A. M. Piechota (2009), Meltwater discharge through the subglacial bed and its land-forming consequences from numerical experiments in the Polish lowland during the last glaciation, *Earth Surf. Processes Landforms*, 34, 481–492.
- Pollard, D., R. M. DeConto, and A. A. Nyblade (2005), Sensitivity of Cenozoic Antarctic ice sheet variations to geothermal heat flux, *Global Planet. Change*, 49(1–2), 63–74.
- Pollard, D., R. M. DeConto, and R. B. Alley (2015), Potential Antarctic Ice Sheet retreat driven by hydrofracturing and ice cliff failure, *Earth Planet. Sci. Lett.*, 412, 112–121.
- Price, P. B., O. V Nagornov, R. Bay, D. Chirkin, Y. He, P. Miocinovic, A. Richards, K. Woschnagg, B. Koci, and V. Zagorodnov (2002), Temperature profile for glacial ice at the South Pole: Implications for life in a nearby subglacial lake., *Proc. Natl. Acad. Sci. U. S. A.*, 99(12), 7844–7847.
- Rajaram, M., S. P. Anand, K. Hemant, and M. E. Purucker (2009), Curie isotherm map of Indian subcontinent from satellite and aeromagnetic data, *Earth Planet. Sci. Lett.*, 281(3–4), 147–158.
- Rignot, E., J. Mouginot, and B. Scheuchl (2011), Ice flow of the Antarctic Ice Sheet, *Science*, 333, 1427–1430.
- Sandiford, M., and S. McLaren (2002), Tectonic feedback and the ordering of heat producing elements within the continental lithosphere, *Earth Planet. Sci. Lett.*, 204, 133–150.
- Schroeder, D. M., D. D. Blankenship, D. A. Young, and E. Quartini (2014), Evidence for elevated and spatially variable geothermal flux beneath the West Antarctic Ice Sheet, *Proc. Natl. Acad. Sci. U. S. A.*, 111(25), 9070–9072.
- Sclater, J. G., and P. Christie (1980), Continental stretching: An explanation of the post-mid-cretaceous subsidence of the central North Sea basin, *J. Geophys. Res.*, 85(B7), 3711–3739.
- Shapiro, N. M., and M. H. Ritzwoller (2004), Inferring surface heat flux distributions guided by a global seismic model: Particular application to Antarctica, *Earth Planet. Sci. Lett.*, 223(1–2), 213–224.
- Shepard, M. K., B. A. Campbell, M. H. Bulmer, T. G. Farr, L. R. Gaddis, and J. J. Plaut (2001), The roughness of natural terrain: A planetary and remote sensing perspective, *J. Geophys. Res.*, 106(E12), 32,777–32,795.
- Siegel, J., D. Lizarralde, B. Dugan, and M. Person (2014), Glacially generated overpressure on the New Englandcontinental shelf: Integration of full-waveform inversion and overpressure modeling, *J. Geophys. Res. Solid Earth*, 119, 3393–3409, doi:10.1002/2013JB010278.
- Siegert, M. J., and J. A. Dowdeswell (1996), Spatial variations in heat at the base of the Antarctic ice sheet from analysis of the thermal regime above subglacial lakes, *J. Glaciol.*, 42(142), 501–509.
- Singhal, B. B. S., and R. P. Gupta (2010), *Applied Hydrogeology of Fractured Rocks*, vol. 430, Springer, N. Y.
- Stauffer, P. H. (2006), Flux flummoxed: A proposal for consistent usage, *Ground Water*, 44(2), 125–128.
- Studinger, M., R. E. Bell, W. R. Buck, G. D. Karner, and D. D. Blankenship (2004), Sub-ice geology inland of the Transantarctic Mountains in light of new aerogeophysical data, *Earth Planet. Sci. Lett.*, 220(3–4), 391–408.
- Sun, B., J. C. Moore, T. Zwinger, L. Zhao, D. Steinhage, X. Tang, D. Zhang, X. Cui, and C. Martín (2014), How old is the ice beneath Dome A, Antarctica?, *Cryosphere*, 8, 1121–1128.
- Thoma, M., K. Grosfeld, C. Mayer, and F. Pattyn (2012), Ice-flow sensitivity to boundary processes: A coupled model study in the Vostok Subglacial Lake area, Antarctica, *Ann. Glaciol.*, 53(60), 173–180.
- Turcotte, D. L., and G. Schubert (2002), *Geodynamics*, Cambridge Univ. Press, N. Y.
- Van Liefferinge, B., and F. Pattyn (2013), Using ice-flow models to evaluate potential sites of million year-old ice in Antarctica, *Clim. Past*, 9(5), 2335–2345.
- Waddington, E. (1987), Geothermal heat flux beneath ice sheets, The Physical Basis of Ice Sheet Modelling, in *Proceedings of the Vancouver Symposium*, August 1987, IAHS Publ., 170, 217–226.
- Waples, D. W. (2001), A new model for heat flow in extensional basins: Radiogenic heat, asthenospheric heat, and the McKenzie Model, *Nat. Resour. Res.*, 10(2), 227–238.
- Wessel, P., and W. H. F. Smith (1996), A global, self-consistent, hierarchical, high-resolution shoreline database, *J. Geophys. Res.*, 101(B4), 8741–8743.
- Wilch, E., and T. J. Hughes (2000), Calculating basal thermal zones beneath the Antarctic ice sheet, *J. Glaciol.*, 46(153), 297–310.
- Winkelmann, R., M. A. Martin, M. Haseloff, T. Albrecht, E. Bueler, C. Khroulev, and A. Levermann (2011), The Potsdam Parallel Ice Sheet Model (PISM-PIK)—Part 1: Model description, *Cryosphere*, 5(3), 715–726.
- Wright, A., and M. Siegert (2012), A fourth inventory of Antarctic subglacial lakes, *Antarct. Sci.*, 24(6), 659–664.
- Young, D. A. et al. (2011), A dynamic early East Antarctic Ice Sheet suggested by ice-covered fjord landscapes, *Nature*, 474(7349), 72–75.
- Zwally, H. J., M. B. Giovinetto, M. A. Beckley, and J. L. Saba (2012), Antarctic and Greenland drainage systems, GSFC Cryospheric Sci. Lab. [Available at [http://icesat4.gsfc.nasa.gov/cryo\\_data/ant\\_grn\\_drainage\\_systems.php](http://icesat4.gsfc.nasa.gov/cryo_data/ant_grn_drainage_systems.php).]